

Electronic Supplementary Information for

Relaxation oscillator-realized artificial electronic neurons, their responses, and noise

Hyungkwang Lim,^{a,b} Hyung-Woo Ahn,^a Vladimir Kornijcuk,^{a,c} Guhyun Kim,^{a,b} Jun Yeong Seok,^{a,b} Inho Kim,^a Cheol Seong Hwang,^b and Doo Seok Jeong^{*a}

^aCenter for Electronic Materials, Korea Institute of Science and Technology, 5 Hwarang-ro 14-gil, Seongbuk-gu, 02792 Seoul, Republic of Korea.

^bDepartment of Materials Science and Engineering and Inter-university Semiconductor Research Center, Seoul National University, 1 Gwanak-ro, Gwanak-gu, 08826 Seoul, Republic of Korea.

^cDepartment of Materials Science and Engineer, Seoul National University of Science and Technology, 232 Gongneung-ro, Nowon-gu, 01811 Seoul, Republic of Korea.

*E-mail: dsjeong@kist.re.kr

SI1. Time-dependent circuit calculation

The calculations of the circuit in Fig. 5a were performed following three steps: (i) V_2^{pre} , V_{out}^{pre} , and V_{in}^{post} , (ii) V_1^{post} , (iii) and V_2^{post} and V_{out}^{post} evaluation steps. The first three variables (V_2^{pre} , V_{out}^{pre} , and V_{in}^{post}) related to the presynaptic neuron are described by employing the Kirchhoff's current law at each node as follows:

$$C_1 \frac{dV_2^{pre}}{dt} = \frac{V_{in} - V_2^{pre}}{R_1} - \frac{V_2^{pre} - V_{out}^{pre}}{R_{TS}}, \quad (S1)$$

$$C_P \frac{dV_{out}^{pre}}{dt} = \frac{V_2^{pre} - V_{out}^{pre}}{R_{TS}} - \frac{V_{out}^{pre} - V_{in}^{post}}{R_{syn}} - \frac{V_{out}^{pre}}{R_2}, \quad (S2)$$

and

$$C_{in} \frac{dV_{in}^{post}}{dt} = \frac{V_{out}^{pre} - V_{in}^{post}}{R_{syn}} - \frac{V_{in}^{post}}{R_{in}}, \quad (S3)$$

where R_{in} and C_{in} are the input resistance (5 G Ω) and capacitance of the non-ideal op-amp (2 pF), respectively. Eqn (S1-S3) were numerically solved using the Crank-Nicolson method. The corresponding discrete forms are expressed as

$$\begin{aligned} \frac{C_1}{\Delta t} \left(\square_2^{pre}(t+1) - V_2^{pre}(t) \right) &= \frac{1}{2R_1} \left(V_{in}(t+1) + V_{in}(t) \right) - \frac{1}{2} \left(\frac{1}{R_{TS}} + \frac{1}{R_1} \right) \left(V_2^{pre}(t+1) + \right. \\ & \left. V_2^{pre}(t) \right) + \frac{1}{2R_{TS}} \left(V_{out}^{pre}(t+1) + V_{out}^{pre}(t) \right), \end{aligned} \quad (S4)$$

$$\begin{aligned} \frac{C_P}{\Delta t} \left(V_{out}^{pre}(t+1) - V_{out}^{pre}(t) \right) &= \frac{1}{2R_{TS}} \left(V_2^{pre}(t+1) + V_2^{pre}(t) \right) - \frac{1}{2} \left(\frac{1}{R_{TS}} + \frac{1}{R_{syn}} + \frac{1}{R_2} \right) \left(V_{out}^{pre}(t+1) + \right. \\ & \left. V_{out}^{pre}(t) \right) + \frac{1}{2R_{syn}} \left(V_{in}^{post}(t+1) + V_{in}^{post}(t) \right), \end{aligned} \quad (S5)$$

and

$$\begin{aligned} \frac{C_{in}}{\Delta t} \left(V_{in}^{post}(t+1) - V_{in}^{post}(t) \right) &= \frac{1}{2R_{syn}} \left(V_{out}^{pre}(t+1) + V_{out}^{pre}(t) \right) - \frac{1}{2} \left(\frac{1}{R_{in}} + \frac{1}{R_{syn}} \right) \left(V_{in}^{post}(t+1) + \right. \\ & \left. V_{in}^{post}(t) \right), \end{aligned} \quad (S6)$$

respectively. V_1^{post} was then evaluated by numerically solving eqn (1). Likewise, the equation can be re-written by a discrete formula. Employing the Kirchhoff's current law at each node of

the postsynaptic neuron, V_2^{post} and V_{out}^{post} – describing postsynaptic dynamics – were finally calculated by solving the following equations:

$$C_1 \frac{dV_2^{post}}{dt} = \frac{V_1^{post} - V_2^{post}}{R_1} - \frac{V_2^{post} - V_{out}^{post}}{R_{TS}}, \quad (S7)$$

and

$$\frac{V_2^{post} - V_{out}^{post}}{R_{TS}} = \frac{V_{out}^{post}}{R_2}. \quad (S8)$$

Eqn (S7) and (S8) were numerically solved using the Crank-Nicolson method.

In order to take into consideration random variability in the switching parameters of the TS, the TS was endowed with random parameters (R_{on} , R_{off} , V_{on} , and V_{off}) for each switching cycle, which follow a normal distribution.

SI2. Slew rate effect on postsynaptic activity

The postsynaptic activity v with R_{syn} was examined for different slew rates ($2.5 - 2000 \text{ V ms}^{-1}$) at a gain of 100 by following the same calculation method in section 3.2.4. The results are shown in Figure SI1.

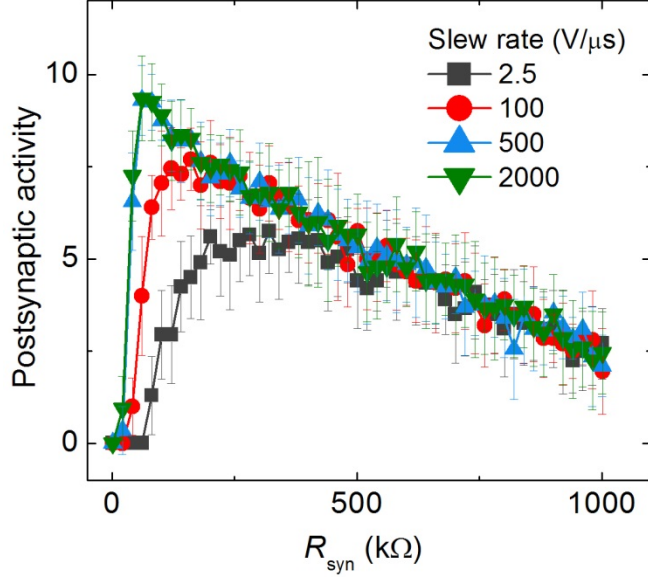


Figure SI1. Postsynaptic activity induced by a presynaptic spike train ($\langle u \rangle = 17.6$) with respect to R_{syn} for different slew rates.

SI3. Activity saturation

The saturation of spiking activity at high V_{in} (Fig. 3) is attributed to saturating ISI. The ISI (spiking period) is mainly determined by the TS's on-state duration (t_{on}) and off-state duration (t_{off}); $\text{ISI} \cong t_{\text{on}} + t_{\text{off}}$. The spiking dynamics in the oscillator was calculated on the circuit in the inset of Figure SI2a in order to elucidate variations in t_{on} and t_{off} in response to V_{in} . The results are plotted in Figure SI2. The employed parameters are shown in Table 1. Spiking behavior at a V_{in} of 6.7 V is shown in Figure SI2a. The spike duration means the TS in the on-state that results in high V_{out} in the oscillator circuit; therefore, t_{on} determines spike width. Given the voltage division through R_1 , TS, and R_2 in series, the abrupt on-switching of the TS lowers V_1 in the circuit in Figure SI2. However, the decrease is rather continuous due to capacitor C_1 , and it continues until $V_{\text{TS}} (=V_1 - V_{\text{out}})$ falls below V_{off} (off-switching voltage of the TS). The immediate

off-switching of the TS elevates V_1 , which is also continuous due to C_1 and continued until V_{TS} reaches V_{on} (on-switching voltage of the TS). This period is referred to as t_{off} as defined beforehand. The described variation in V_1 amid spiking is displayed in Figure SI2b.

The higher V_{in} is applied, the more rapidly V_{TS} rises within t_{off} ; t_{off} is consequently shortened as shown for the two different V_{in} values (4 V and 6.7 V) in Figure SI2d. Higher V_{in} results in higher V_1 in the steady state given the voltage division through R_1 , TS, and R_2 in series irrespective of resistance state of the TS. Recalling capacitor charging in a simple R-C circuit, the voltage across the capacitor (V_c) changes in due course following $V_c = V_{c0}(1 - e^{-t/RC})$, where V_{c0} denotes V_c in the steady state. In order for V_c to reach a certain voltage V_p ($V_p < V_{c0}$), it takes time t_p , $t_p = RC \ln(V_{c0}/(V_{c0} - V_p))$, i.e. the requisite time t_p decreases with increasing steady state voltage V_{c0} . The same holds for charging C_1 in our oscillator within t_{off} , which underlies the decrease of t_{off} with V_{in} .

By contrast, higher V_{in} rather tends to stretch t_{on} to some extent, although the effect is not as substantial as the t_{off} change (see Figures SI2c and d). Given that C_1 is discharged within t_{on} , capacitor discharging in a simple R-C circuit can be invoked for the period t_{on} . While discharging, V_c decays with time towards the steady state value, and the V_c decay rate largely decreases in the vicinity of the steady state voltage. V_1 in the oscillator likewise decays through the period t_{on} towards V_1 in the steady state, and it crosses $V_{off} + V_{out}$, resulting in the off-state of the TS. Also, the decay rate declines as V_1 becomes close to the steady state V_1 . The steady state V_1 is elevated with V_{in} , and thus the requisite time for reaching $V_{off} + V_{out}$ slightly increases with V_{in} as shown in Figures SI2c and d. Figure SI2e clearly uncovers the effect of V_{in} on t_{on} , t_{off} , and ISI ($t_{on} + t_{off}$), and the consequent saturation of ISI at high V_{in} . Therefore, the saturation of

spiking activity, parameterized by the number of spikes, is eventually achieved at high V_{in} (Figure SI2f).

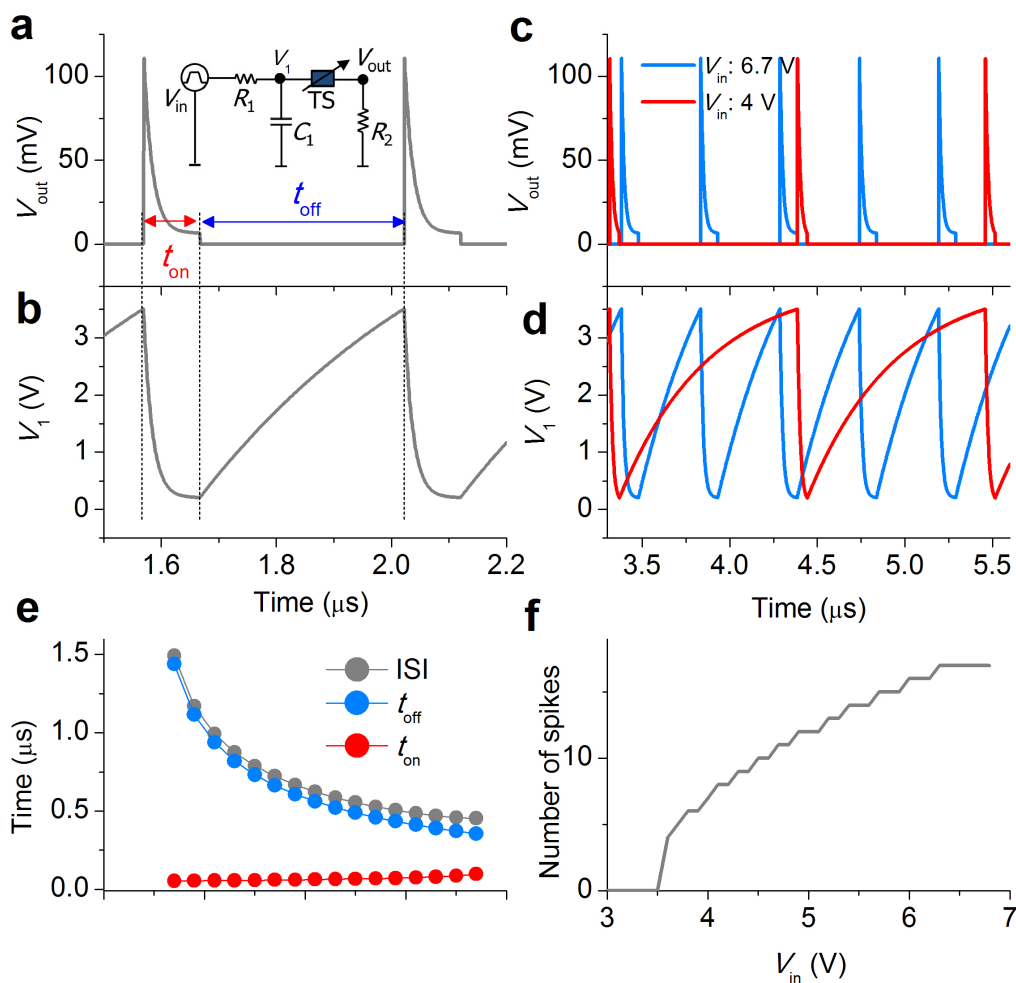


Figure SI2. (a) Simulated spiking behavior ($V_{in} = 6.7$ V) in the oscillator shown in the inset. t_{on} and t_{off} indicate on- and off-state duration in the TS, respectively. (b) Simultaneous variation in V_1 with V_{out} in (a). (c) Spiking behavior at two different V_{in} values (4 V and 6.7 V) and (d) the corresponding V_1 variation. (e) Change of t_{on} , t_{off} , and spiking period (ISI), i.e. $t_{on}+t_{off}$, upon V_{in} . (f) Variation in the number of spikes with respect to V_{in} .

SI4. Threshold switch fabrication

The crossbar-type TS cells were fabricated as follows. First, a blanket Pt bottom electrode (50 nm) was deposited on a Si wafer with a Ti adhesion layer (10 nm) underneath the Pt layer by using electron-beam evaporation. The blanket bottom electrode layer was patterned by means of a standard photolithography technique. We subsequently deposited a GeSe layer (100 nm) onto the patterned bottom electrode by using an rf magnetron co-sputtering unit with separate Ge₄Se₆ and Ge targets. During sputtering, the rf-power applied to the Ge₄Se₆ and Ge targets (30 and 20 W, respectively), and working pressure (0.5 mTorr) were maintained, which yielded a deposition rate of 12.2 nm/min). Finally, a blanket Pt top electrode (50 nm) was deposited onto the GeSe layer by using electron-beam evaporation and patterned in the same way as for the bottom electrode. The cross-point area was set to 5×5 μm².